

Structural, electronic, and magneto-optical properties of  $\text{YVO}_3$ 

A. A. Tsvetkov, F. P. Mena, P. H. M. van Loosdrecht, and D. van der Marel

Materials Science Center, University of Groningen,  
Nijenborgh 4, 9747 AG Groningen, The Netherlands

Y. Ren

Experimental Facilities Division, Advanced Photon Source,  
Argonne National Laboratory, Argonne, IL 60439A. A. Nugroho<sup>y</sup>Solid State Chemistry Lab, MSC, University of Groningen,  
Nijenborgh 4, 9747 AG Groningen, The Netherlands

A. A. Menovsky

Van der Waals – Zeeman Institute,  
University of Amsterdam, Valckenierstraat 65,  
1018 XE Amsterdam, The Netherlands

I. S. Elmov and G. A. Sawatzky

Department of Physics and Astronomy,  
The University of British Columbia,  
334-6224 Agricultural Rd., Vancouver, B.C. V6T 1Z1 Canada

(Dated: April 14, 2024)

## Abstract

Optical and magneto-optical properties of  $\text{YVO}_3$  single crystal were studied in FIR, visible, and UV regions. Two structural phase transitions at 75 K and 200 K were observed and established to be of the first and second order, respectively. The lattice has an orthorhombic  $Pbnm$  symmetry both above 200 K as well as below 75 K, and is found to be dimerized monoclinic  $Pb11$  in between. We identify  $\text{YVO}_3$  as a Mott-Hubbard insulator with the optical gap of 1.6 eV. The electronic excitations in the visible spectrum are determined by three d-bands at 1.8, 2.4, and 3.3 eV, followed by the charge-transfer transitions at about 4 eV. The observed structure is in good agreement with LSDA+U band structure calculations. By using ligand field considerations, we assigned these bands to the transitions to the  $^4A_{2g}$ ,  $^2E_g + ^2T_{1g}$ , and  $^2T_{2g}$  states. The strong temperature dependence of these bands is in agreement with the formation of orbital order. Despite the small net magnetic moment of 0.01  $\mu_B$  per vanadium, the Kerr effect of the order of 0.01 was observed for all three d-bands in the magnetically ordered phase  $T_{N\text{eel}} < 116\text{K}$ . A surprisingly strong enhancement of the Kerr effect was found below 75 K, reaching a maximum of 0.1. The effect is ascribed to the non-vanishing net orbital magnetic moment.

PACS numbers: 71.20.-b, 78.20.-e, 78.30.-j

## I. INTRODUCTION

The interplay between kinetic energy and Coulomb interaction in strongly correlated electron systems enables small external or internal perturbations to manipulate electronic and magnetic properties of the matter. If, in addition, there is a ground state degeneracy, further interesting phenomena, like an orbital ordering can arise<sup>1</sup>.

In yttrium orthovanadate,  $\text{YVO}_3$ , spin and orbital ordering was suggested to be responsible for at least one of the temperature induced sign reversals of magnetization<sup>2</sup>. In the magnetically ordered phase,  $\text{YVO}_3$  is a canted antiferromagnet, where a net ferromagnetic moment is formed by a small angle between the antiferromagnetically (AFM) oriented spins of  $\text{V}^{3+}$  ions. The transition from the room temperature paramagnetic phase to the antiferromagnetic state occurs at the Neel temperature  $T_N = 116 \text{ K}$ . Upon further lowering the temperature, the magnetic moment gradually changes sign around  $90 \text{ K}$ . It has been argued that this magnetization reversal is due to the opposing effects of the Dzyaloshinsky-Moriya interaction and the single-ion magnetic anisotropy on the spin canting direction<sup>2</sup>. The magnetization switches sign again around  $77 \text{ K}$ . At this temperature the antiferromagnetic order changes from the high temperature C type to the low temperature G type<sup>3</sup>. A C-type AFM order corresponds to an AFM arrangement in planes and a ferromagnetic arrangement between the planes. A G-type AFM order implies completely antiferromagnetic arrangement, both within planes and between them. Ren et. al.<sup>2</sup> argued that along with the spin order there is an orbital order on the vanadium sites. According to the proposed picture, one of two 3d electrons always occupies the xy orbital, while another electron occupies alternatively either the xz or yz orbital on different atoms, thus forming orbital order. In order to minimize the exchange energy a C-type spin order is accompanied by a G-type orbital order and vice versa. The onset temperature of the orbital order was reported to be much higher than the Neel temperature,  $T_{O_O} = 200 \text{ K}$ <sup>4</sup>.

The proposed picture of the electronic structure still requires confirmation from, for instance, spectroscopic experiments. The strength of optical transitions involving a charge transfer between orbitals of different ions should be highly susceptible to orbital order between the ions. Indeed, one of the aims of the present research is to study the influence of orbital ordering on optical transition strengths, and use this technique to study orbital ordering in  $\text{YVO}_3$ . In this paper we present, amongst others, optical and magneto-optical

measurements of electronic excitations in  $\text{YVO}_3$  single crystals. The observed electronic spectra are discussed using ligand field theory considerations and compared to LDA+U calculations. In addition, magneto-optical Kerr effect experiments are used to elucidate the spin orientation.

The crystal structure of yttrium orthovanadate  $\text{YVO}_3$  was initially reported to have an orthorhombic  $\text{Pbnm}$  ( $\text{D}_{2h}^{16}$  in Schoenflies notation) symmetry at all temperatures<sup>5,6</sup>. Recent synchrotron measurements<sup>4,7</sup> report the observation of an additional (401) reflection below 200 K, inconsistent with the  $\text{Pbnm}$  symmetry. The authors concluded<sup>4</sup> that the crystal structure was most likely  $\text{P2}_1=\text{a}$ , the highest symmetry subgroup of  $\text{Pbnm}$ . However, the intensity of the  $\text{Pbnm}$  forbidden reflection was four orders of magnitude weaker than to the allowed reflection<sup>4</sup>, which seemed to make the refinement of the X-ray data very difficult. Far infrared (FIR) spectroscopy is a very sensitive tool to study crystal structure variations. Minor atomic displacements due to a symmetry breaking, which may be difficult to elicit from x-ray analysis, manifest itself through the appearance of new phonon lines in the FIR spectrum. Recently, Ulrich et. al.<sup>8</sup> proposed that  $\text{YVO}_3$  can be subjected to a new sort of Peierls instability, where the new ground state involves a dimerization along the c axis. From the crystallographic and optical points of view this dimerization removes the inversion center, and IR and Raman active phonons become mixed. The a-axis modes stays nevertheless independent from the b or c axes, if the dimerization affects only the c axis. We use the FIR vibrational spectroscopy to follow temperature induced variations of the phonon spectrum and to refine the crystal structure of  $\text{YVO}_3$ .

## II. EXPERIMENTAL DETAILS

Polycrystalline powder of  $\text{YVO}_3$  was prepared from  $\text{YVO}_4$  powder as starting material. The  $\text{YVO}_4$  powder was prepared by a high temperature solid-state reaction from appropriate mixtures of pre-dried  $\text{Y}_2\text{O}_3$  (99.998 %) and  $\text{V}_2\text{O}_5$  (99.995 %, metal basis). The oxygen in  $\text{YVO}_4$  was reduced by annealing the powder in a flow of pure  $\text{H}_2$  at 1000 C. The growth process was carried out by the coating zone technique using a four-mirror furnace in a flow of Ar gas<sup>9</sup>. The single-crystalline boule of about 6 mm in diameter and 60–70 mm in length was obtained from the growth. The crystallinity of the boule was checked by Laue X-ray diffraction. The elemental composition of the crystal was checked by the electron probe

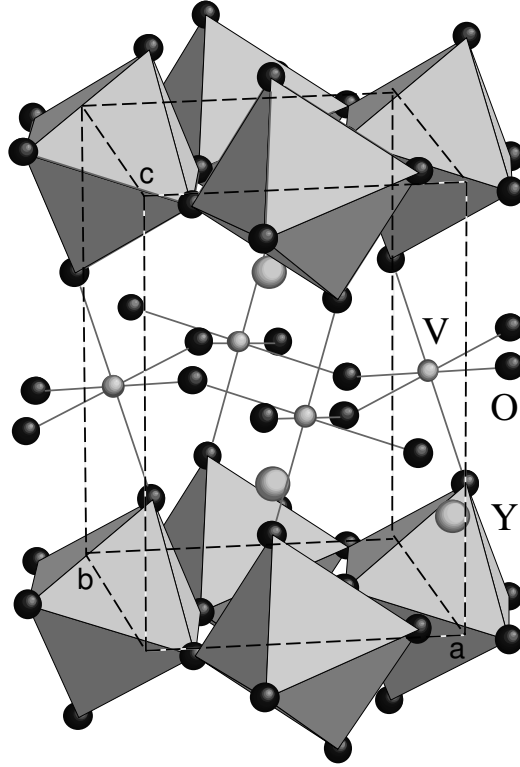


FIG. 1: Pbnm orthorhombic crystal structure of  $\text{YVO}_3$ .

micro analyzer (EPMA) and the results showed that the molar ratios were given by  $\text{Y:V:O} = 1.00:1.00:3.02$ . A separate check of the composition using the chemical analysis method showed that the cation ratio of Y over V was  $1.00 \pm 0.01$  and that the oxygen stoichiometry was  $3.03 \pm 0.02$ . Both results were in good agreement.

The dielectric function for near-infrared, visible, and ultra-violet spectral ranges was obtained directly by using the ellipsometry technique. Because ellipsometric measurements are very sensitive to contamination of the surface, we used an ultra-high vacuum cryostat with a residual pressure less than  $10^{-8}$  mbar. The cryostat was specially designed to minimize the movements of the sample due to the thermal expansion of the cold finger. The spectra were measured with a VASE 32 ellipsometer from J.A. Woollam Co., Inc., covering a spectral range from  $6000 \text{ cm}^{-1}$  through  $36000 \text{ cm}^{-1}$  ( $0.75\text{--}4.5 \text{ eV}$ ).

Far-infrared and mid-infrared reflectivity spectra were measured by Fourier Transform Infrared reflection spectroscopy using a Bruker IFS-113v. The intensity of the reflected light from the sample was referenced to that from a gold mirror for every measured optical surface at each polarization. The sample was mounted on the cold finger of a helium flow cryostat,

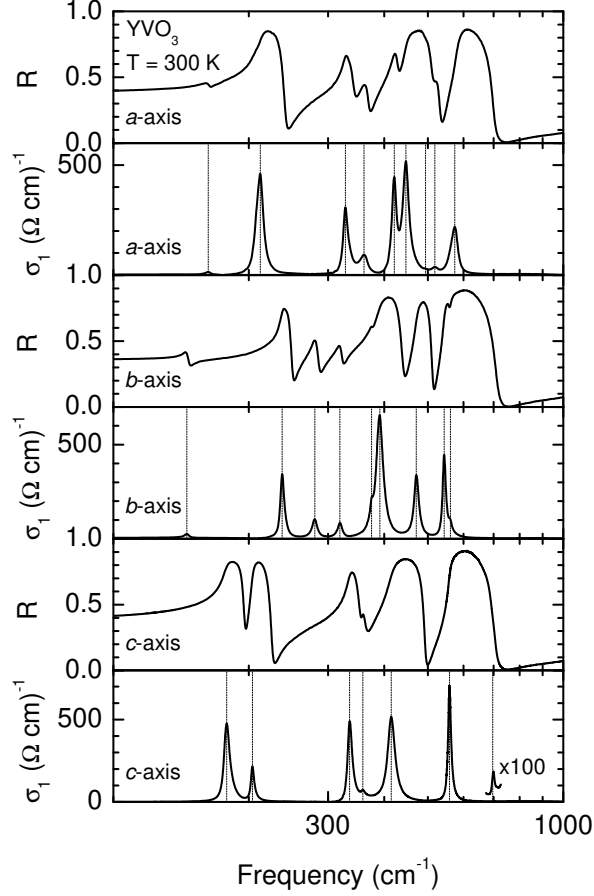


FIG. 2: The room temperature reflectivity and corresponding optical conductivity for the three crystallographic directions. Dashed lines indicate position of the phonon modes. There are 9, 9, and 7 modes for the  $a$ ,  $b$ , and  $c$  axes, respectively, in agreement with the  $Pbnm$  symmetry.

whose temperature was varied from 300 K down to 4.2 K. Kramers-Kronig transformation was used to calculate the dielectric function and optical conductivity from the reflectivity data in the infrared region. For these calculations we extrapolated the reflectivity below 50  $\text{cm}^{-1}$  with a pure ionic insulator response. For the high frequency extrapolation we used the reflectivity calculated from the ellipsometric data.

The magneto-optical properties were measured using a home-built Kerr spectrometer. We used the electro-optical modulation technique, similar to [10], to obtain simultaneously the Kerr rotation and ellipticity induced by the sample. The combination of Xenon arc lamp, windows, Si-detector, and other optical components limited our spectral range to the band from 350 nm through 800 nm (1.55–3.5 eV).

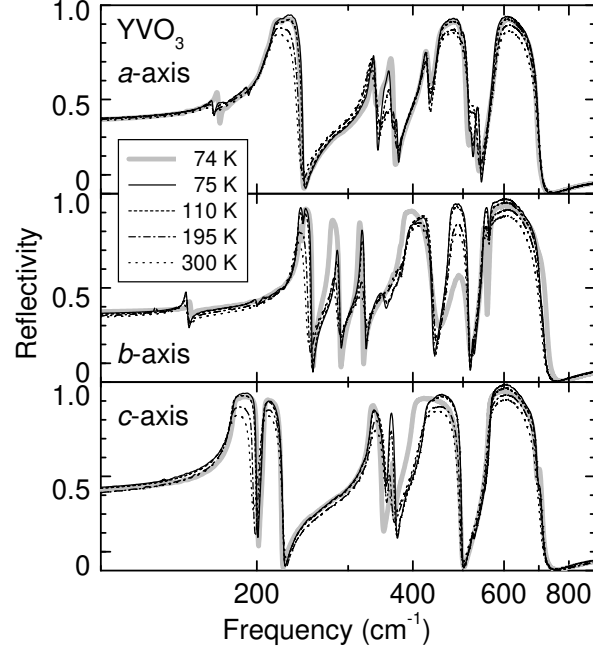


FIG. 3: Temperature dependence of the FIR reflectivity for three polarizations.

### III. STRUCTURAL PHASE TRANSITIONS

The orthorhombic  $Pbnm$  crystal structure of  $YVO_3$  is shown in Fig. 1. It can be considered as a distorted perovskite structure. When compared to the perovskite unit cell, the orthorhombic  $a$  and  $b$  axes lay along the diagonals of the perovskite unit cell and the corresponding translational vectors are approximately  $\frac{1}{\sqrt{2}}$  times longer. The  $c$ -axis dimension of the orthorhombic unit cell is twice as large. The  $YVO_3$  unit cell contains thus four formula units. Vanadium ions have an octahedral surrounding. The octahedrons are distorted, rotated and tilted with respect to each other, as illustrated in Fig. 1.

In the present work we use optically active phonons to track changes in the crystal symmetry. As yttrium orthovanadate is an insulating compound, its optical response in the far-infrared (FIR) region is determined purely by lattice vibrations. In Fig. 2 the room temperature reflectivity for all three polarizations is shown together with the optical conductivity. As can be seen, there are 9, 9, and 7 optically active modes respectively for the  $a$ ,  $b$ , and  $c$  axes. The positions of the TO phonon frequencies are shown by vertical lines and the frequencies are given in Tables I and II. Some resonances are very weak. For example, the mode of highest frequency for the  $c$  axis is hardly visible in the conductivity and appears as a shoulder on the reflectivity curve. It gains intensity as the temperature is lowered, and

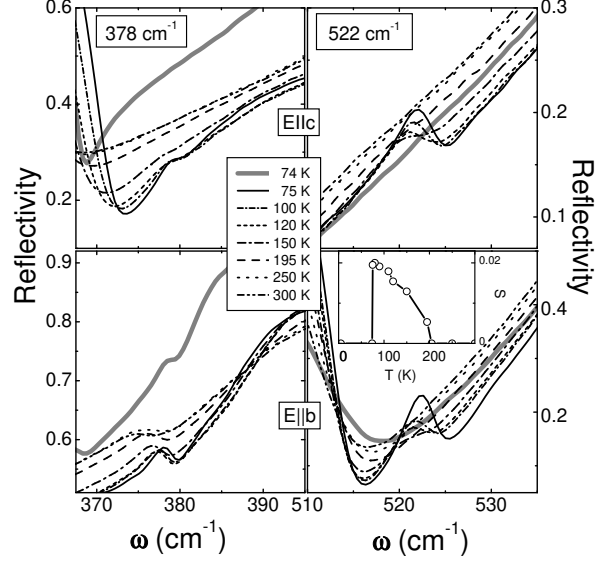


FIG. 4: Left panels: "Leakage" of the b-axis  $B_{3u}$  mode into the c-axis response. Right panels: Appearance of a new previously silent  $A_u$  mode in the b and c responses. Insert: Temperature dependence of the optical strength of the new mode.

reaches its maximum in the low temperature orthorhombic phase. Shown in Fig. 3 is the temperature dependence of the reflectivity for all three polarizations. The number of the phonons stays the same between room temperature and 200 K. Below 200 K a number of additional phonons gradually emerges. We illustrate this by picturing some of the new modes for the b and c axes in Fig. 4. As can be seen from the figure, the intensity of the new modes evolves continuously and monotonically as the temperature decreases, reaching its maximum at 75 K. The optical strengths remain however one or two orders of magnitude weaker than that of the original main modes. Below 75 K the new phonons discontinuously disappear. As an example, the temperature dependence of the oscillator strength of the new 522  $\text{cm}^{-1}$  mode is shown in Fig. 4.

To analyze the observed phonon spectra, we apply a group theory analysis. The primitive cell of  $\text{YVO}_3$  contains four formula units, yielding 60 phonon modes in total. In the Pbnm lattice the four yttrium atoms and four vanadium atoms occupy equivalent sites 4c and 4b in Wyckoff notation with the site symmetry  $C_s^{xz}$  and  $C_1$ , respectively. The 12 oxygen atoms are distributed between two inequivalent sites 4c and 8d with the site symmetry  $C_s^{xz}$  and  $C_1$ , respectively. Using the general procedure,<sup>11</sup> we find that the phonon normal modes



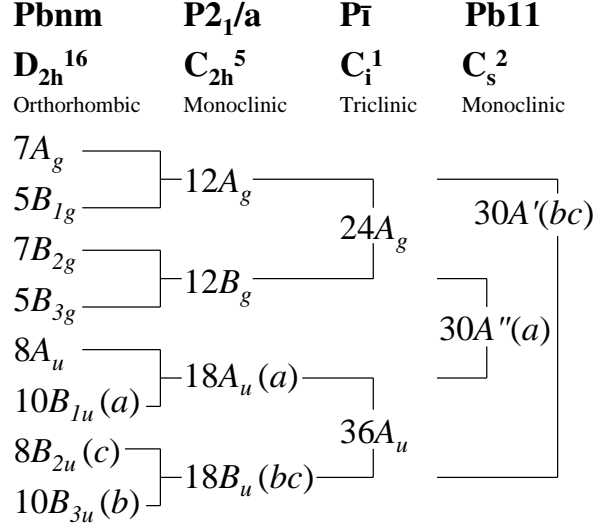


FIG. 5: Transformations of the phonon irreducible representations due to the descent in lattice symmetry.

transform like 60 irreducible representations

$$= 7A_g + 8A_u + 5B_{1g} + 10B_{1u} + 7B_{2g} + 8B_{2u} + 5B_{3g} + 10B_{3u} :$$

The total representation can be subdivided into three acoustic vibrational modes,  $B_{1u} + B_{2u} + B_{3u}$ , 24 Raman active modes,  $7A_g + 5B_{1g} + 7B_{2g} + 5B_{3g}$ , eight silent  $A_u$  modes, and 25 infrared active modes. The infrared vibrations are split into  $9B_{1u}$  (E<sub>g</sub>),  $9B_{3u}$  (E<sub>g</sub>), and  $7B_{2u}$  (E<sub>g</sub>) modes with the electric dipole moment aligned along the *a*, *b*, and *c* axes, respectively.

A similar group theory analysis is applied to the lower symmetry structures,  $P2_1/a$ ,  $P\bar{1}$ , and  $Pb11$ , which are sub-groups of the  $Pbnm$  symmetry. Table III illustrates which symmetry elements are inherited in different symmetries. We also show a relation between the widely used notation  $Pbnm$ , adopted also in this paper, and the standard notation  $Pnma$ . The monoclinic  $P2_1/a$  symmetry is postulated from the X-ray measurements<sup>7</sup>. The triclinic  $P\bar{1}$  symmetry, second highest possible symmetry after  $P2_1/a$ , was proposed by us for the case, when the center of inversion is conserved<sup>12</sup>. Both x-ray<sup>7</sup> and optical measurements<sup>12</sup> show that the symmetry can not be higher than monoclinic. Recent neutron experiments indicated the possibility of a dimerized state<sup>8</sup>. Dimerization displaces the middle  $VO_2$  plane, see Fig. 1, away from its central position. It removes the inversion center and screw axis from the symmetry operations of  $P2_1/a$ . The remaining symmetry group includes only a

glide plane  $b$  and is referred as  $Pb11$ .

As the X-ray measurements do not reveal any multiplication of the unit cell,<sup>4</sup> the number of the atoms in the unit cell is not changed. For monoclinic  $P2_1/a$  ( $C_{2h}^5$ ) symmetry group one expects  $16B_u$  IR active and 2 acoustic modes in the  $bc$  plane and  $17A_u$  IR and one acoustic modes along the  $a$  axis. In case of triclinic  $P\bar{1}$  ( $C_i^1$ ) symmetry, there should be  $33A_u$  IR modes, which can have components along all the three axes. Monoclinic  $Pb11$  ( $C_s^2$ ) symmetry splits phonons into two irreducible representations  $30A^0(E_{jbc}) + 30A^0(E_{j\bar{a}})$ , where Raman and IR modes are mixed. The way how the phonon modes' irreducible representations transform into each other due to the descent in symmetry is depicted in Fig. 5. Both monoclinic  $C_{2h}^5$  and triclinic  $C_i^1$  crystal lattices have an inversion center. As a result the IR and Raman modes do not mix with each other for these symmetries. In point group  $C_{2h}$ , because the  $b$  and  $c$  axes are not orthogonal any more, the corresponding phonons mix and form the  $B_u$  representation,  $7B_{2u} + 9B_{3u} \rightarrow 16B_u$ . The mode  $A_u$ , silent in  $D_{2h}^{16}$  symmetry, becomes optically active and together with the  $B_{1u}$  mode gives the  $A_u$  representation,  $8A_u + 9B_{1u} \rightarrow 17A_u$ . A possible twinning in the  $b-c$  plane cannot be a reason for leaking the  $b-c$  phonons to the  $a$  axis and vice versa. Alternatively, in the lowest  $C_i^1$  symmetry all the phonons mix together, as seen in Fig. 5. In the  $Pb11$  symmetry, Raman  $A_g$  modes become visible in the  $bc$  plane and together with the IR  $B_u$  phonons form the  $A^0$  representation,  $12A_g + 18B_u \rightarrow 30A^0$ . Similar, Raman  $B_g$  modes can be observed in the  $a$  axis response together with IR  $A_u$  modes,  $12B_g + 18A_u \rightarrow 30A^0$ . An important difference between  $P\bar{1}$  and  $Pb11$  symmetries is that in  $P\bar{1}$  the same modes can be observed in all three polarizations, while in  $Pb11$   $a$  eigenmodes on one side and  $b$  and  $c$  eigenmodes on the other side remain separate.

At room temperature we observed 9, 9, and 7 phonons for the  $a$ ,  $b$ , and  $c$  axes, respectively (see Fig. 2). The TO phonon frequencies  $\omega$ , broadening  $\gamma$  and optical strength  $S$  are presented in Tables I and II. Our observation confirms the orthorhombic  $Pbnm$  symmetry of the crystal lattice at room temperature. At lower temperatures, as far as the crystal structure is concerned, we can conclude from Fig. 4 that the  $Pbnm$  symmetry is transformed to a lower one below 200 K and it is restored again below 75 K. Evolution of the optical strength of the new phonons with temperature indicates that the transition at 200 K is restored again below 75 K. The temperature evolution of the optical strength of the new phonons indicates that the phase transition at 200 K has a second order nature and

that the one at 75 K has a first order nature. Shown in Table II are the phonon mode frequencies and strengths observed in the c axis spectrum at 75 K. The lines active also in the high temperature phase are in bold face and assigned to  $B_{2u}$ , those appearing only in the intermediate temperature phase are labelled by A. Although much more new phonons are seen for all three axes, only the activated c-axis modes, having a counterpart in the other axes, are shown in the table. First, one can see that the original c-axis phonon lines give rise to phonon absorptions along the b axis. The reverse is also valid. The phonons from the b axis 'leak' in the intermediate phase to the c axis, which is shown in Fig. 4. This agrees with all three symmetries under consideration. However, there is a number of newly activated absorption peaks (199, 350, and 522  $\text{cm}^{-1}$ ) in the b and c polarizations, which do not have parents in other polarizations. The fact that these new modes are exactly at the same frequency in both b and c polarizations – as shown in the right panels of Fig. 4 – exclude the possibility of the doubling of the unit cell as their origin. The appearance of new modes is forbidden in the  $P2_1/a$  symmetry (see also Fig. 5). This observation rules out the  $P2_1/a$  symmetry for the intermediate phase. Because these modes are not seen in any polarization above 200 K or below 75 K, we can ascribe these phonons either to the previously silent mode  $A_u$  activated in the  $P\bar{1}$  symmetry or to the high temperature Raman modes activated in  $Pb11$  symmetry. We did not observe any correlation of phonons between b and c on one side and a on the other side, apart from the modes already present both in a and c polarizations above 200 K, 333 and 420  $\text{cm}^{-1}$  modes in Table II. This could imply that the triclinic distortions are extremely small, in particular for the a axis. However, the  $Pb11$  symmetry gives a more natural explanation, as it keeps the a and bc modes apart consistent with the observation. All in all, these facts draw us to the conclusion that the crystal structure of  $\text{YVO}_3$  in the intermediate phase most likely has a monoclinic  $Pb11$  symmetry. A further test for this conclusion could be a comparison to Raman measurements, when data becomes available.

Finally, we remark on the relation between the electronic and crystal structure changes. From Fig. 6 one can see that the main modes evolve smoothly through the second order phase transition, where the appearance of the orbital order is reported<sup>4,7</sup>. However, modes change their frequency substantially at the first order phase transition changes some, where spins and orbitals switch their ordering. The frequency change is found to be particularly strong for the modes around 400  $\text{cm}^{-1}$ . From lattice dynamical calculations<sup>13</sup> for the isostructural

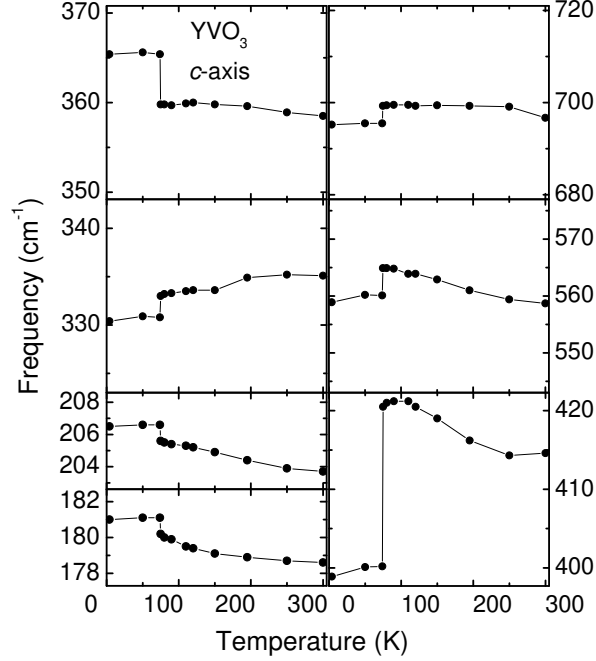


FIG . 6: Temperature dependence of the TO frequencies for the c-axis  $B_{2u}$  phonon modes. For comparison purposes, vertical scale in each square comprises 6% of the central frequency.

compound  $\text{LaMnO}_3$  we conclude that the  $400 \text{ cm}^{-1}$  modes mainly involve vanadium-oxygen bond vibrations. Therefore, it seems that the main structural changes at the first order transition involve a distortion of the  $\text{VO}_6$  octahedra.

#### IV . ELECTRONIC STRUCTURE

The yttrium  $\text{Y}^{3+}$  and vanadium  $\text{V}^{3+}$  ions in  $\text{YVO}_3$  both carry the formal charge  $3+$ . Yttrium has a complete shell, and it can be excluded from the consideration for the electronic transitions. Vanadium has two 3d electrons in the outer shell. We can thus expect two types of optical transitions in the visible range: d-d transitions between vanadium ions with the characteristic energy of the Motz-Hubbard gap (Motz-Hubbard (MH) transitions), and the charge-transfer (CT) transitions from the oxygen 2p-band to the free states in the vanadium 3d-band.

Shown in Figs. 7 and 8 are the real and imaginary parts of the  $\text{YVO}_3$  dielectric function,  $\epsilon = \epsilon'' + i\epsilon''$ , measured at various temperatures. The optical response at low temperatures is determined by three bands with their maxima located at 1.8, 2.4, and 3.3 eV, followed

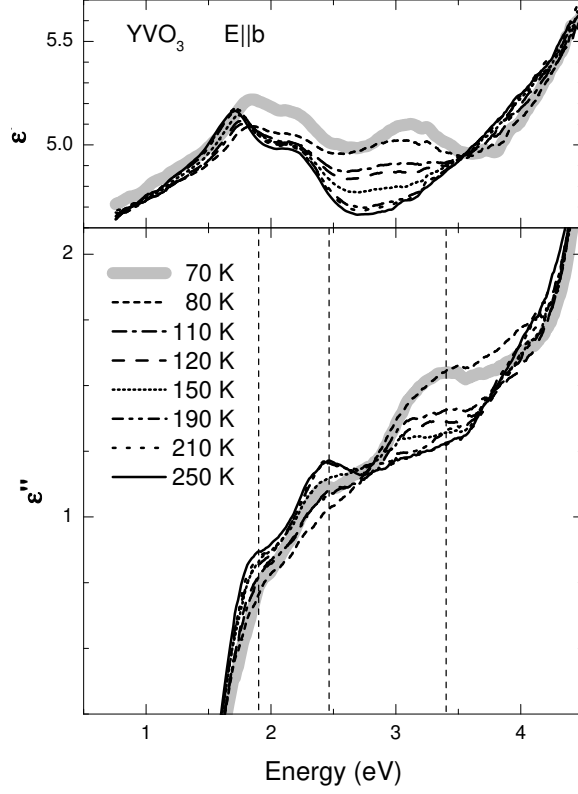


FIG . 7: Temperature dependence of the real and imaginary part of the b-axis dielectric function for  $\text{YVO}_3$ . The vertical lines indicate locations of the band maxima.

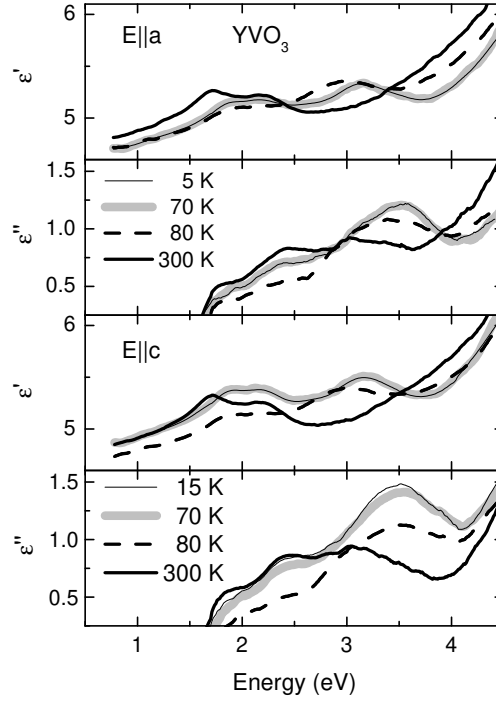


FIG . 8: The real and imaginary part of the dielectric function for the a- and c-axes of  $\text{YVO}_3$ .

by a sharp upturn above 4 eV. The optical gap is found at 1.6 eV. It is quite remarkable to observe that the intensity of some bands, located in the region of a few electron-volts, changes by as much as 50% for temperature variations as low as  $k_B T = 26$  meV.

Recently Miyasaka et. al.<sup>14</sup> reported reflectivity measurements on  $YVO_3$ , where the optical conductivity, obtained through the Kramers-Kronig relations, revealed only two peaks. Also the temperature dependence and the reported anisotropy of the conductivity were different. Since  $\epsilon''$  is approximately five times smaller than  $\epsilon'$  in the visible part of the spectrum, the reflectivity is mainly determined by the real part of  $\epsilon$ . The d-band structure in  $\epsilon'$  and  $\epsilon''$  gives rise to the corresponding reflectivity variations of only few percent and the temperature induced changes of the reflectivity are around 1% or less. This together with the close vicinity of the strong charge transfer transitions place heavy demands on the accuracy of the measurements. A small error can substantially affect an interpretation of the electronic spectrum. We used the ellipsometric technique, which determined  $\epsilon'$  and  $\epsilon''$  directly at each particular photon energy and excluded the necessity of reference measurements. In addition we took special precautions to perform measurements in ultra-high vacuum in order to avoid condensation on the surface at low temperatures. We trust that these measures minimize a possible error.

Let us first discuss the origin of the bands. Following the general classification scheme<sup>15</sup>,  $YVO_3$  is a Mott-Hubbard insulator. The lowest excitations are  $d_i^2 d_j^2 \rightarrow d_i^3 d_j^1$  transitions between different vanadium ions,  $i$  and  $j$ . The upturn above 4 eV is due to charge transfer excitations. This general picture follows from our LSDA+U calculations and agrees with previous room temperature measurements<sup>16,17</sup>. The fine structure of the MH band observed here has not been reported previously and will be discussed using ligand field theoretical considerations and LSDA+U calculations.

Because the orthorhombic distortion of the oxygen octahedron is small, we can neglect any on-site d-d excitations. For the same reason we can, considering the energy diagram, restrict ourselves in the first approximation to the  $O_h$  symmetry on the vanadium site. The  $e_g$  orbitals can be excluded, because due to the large crystal field splitting,  $10Dq$ , the mixing between  $e_g$  and  $t_{2g}$  orbitals is expected to be small. Thus, in the strong field approximation the two d electrons occupy  $t_{2g}$  orbitals.

If we take into account the Coulomb interaction, the  $t_{2g}$  level is split into  $^3T_{1g}$ ,  $^1E_g$ ,  $^1T_{2g}$ , and  $^1A_{1g}$  levels, as shown in Fig. 9 (a). The  $^1E_g$  and  $^1T_{2g}$  levels are degenerate in

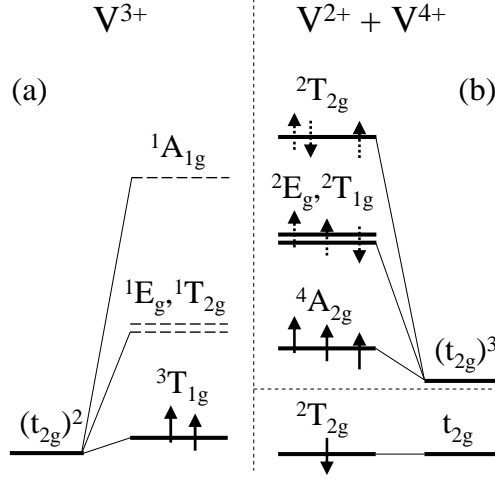


FIG. 9: Energy diagram for (a) the ground state of the vanadium ions and (b) excited states of two vanadium sites.

the  $O_h$  symmetry. In the ground state the d electrons occupy the lowest energy  $S=1$  state,  $^3T_{1g}$ , in agreement with the Hund's rule. The MH excitations occur from the initial state with two vanadium in the  $d^2$  state to the final state with the first atom in the  $d^1$  ( $V^{4+}$ ) and the second in the  $d^3$  ( $V^{2+}$ ) states. In the final state the wave function of the single electron follows obviously only one irreducible representation  $^2T_{2g}$ , while the  $d^3$  state splits into four levels,  $^4A_{2g}$ ,  $^2E_g$ ,  $^2T_{1g}$ , and  $^2T_{2g}$ , with  $^2E_g$  and  $^2T_{1g}$  again being degenerate. The energy diagram of the final state is depicted in Fig. 9 (b). The three observed bands in Fig. 7 correspond to transitions to these three energy levels. According to the measurements, these bands span the energy range of 1.5 eV from 1.8 eV to 3.3 eV. With the crystal field splitting of  $10Dq \approx 2$  eV, our assumption of a small admixture of  $e_g$  orbitals is justified.

The picture obtained with the ligand field theory is in good agreement with our LSDA + U calculations. The LSDA + U band structure calculations have been performed in the LMTO calculation scheme<sup>18,19</sup>. Vanadium 3d partial density of states were obtained in the LDA + U calculation with  $U = 3.4$  eV and  $J = 0.85$  eV for the low temperature crystal and magnetic structure of  $YVO_3$ . The results are consistent with previous calculations of the electronic structure<sup>20</sup>. As can be seen from the electron density of states in Fig. 10, the highest occupied states are from a narrow d band, with both electrons in a spin-up state. The AFM ordered neighboring vanadium ion should be accordingly in a spin-down state. The lowest unoccupied band corresponds to the addition of an electron with spin up. This agrees with

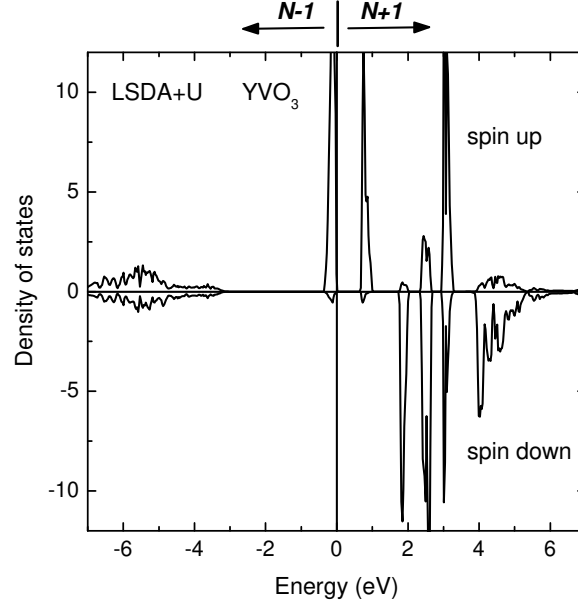


FIG. 10: Vanadium 3d partial density of states for spin-up and spin-down electrons, obtained in local spin-density approximation with the Hubbard potential  $U$  taken into account.  $N-1$  and  $N+1$  correspond to the electron removal and electron addition states, respectively.

the lowest excited  ${}^4A_{2g}$  state, which indeed puts electrons in the high-spin state  $S = 3/2$ . Two consequent excitation bands are formed by transfer of spin-down electrons, again in agreement with the low  $S = 1/2$  spin states in the  ${}^2E_g$ ,  ${}^2T_{1g}$ , and  ${}^2T_{2g}$  representations found from the ligand field theory. Higher electron-addition bands with equal spin-up/spin-down populations have an  $e_g$  origin. From the energy distribution of the bands in Fig. 10 one can see that  $YVO_3$  is indeed a Mott-Hubbard insulator<sup>15</sup>. The lowest excitations are  $d-d$  transitions,  $d^2d^2 \rightarrow d^3d^1$ . The charge-transfer transitions,  $d^2 \rightarrow d^3\bar{L}$  occur at higher energies than the  $d-d$  transitions.

The temperature dependence of the optical response of  $YVO_3$  is shown in Figs. 7 and 8. There is only small  $T$ -dependence between 70 K and 6 K, as can be seen in Fig. 8, and the corresponding data are further omitted from the consideration. To clarify the temperature dependence of the MH bands, Fig. 11 shows a differential dielectric function for  $E_{\parallel}$ , where the 250 K data are subtracted from the curves in Fig. 7. In order to quantify temperature variations of the optical strength of the bands, we fitted simultaneously the real and imaginary parts. The differential dielectric function turned out to be well fitted with three gaussians in the imaginary part and with its Hilbert transform, Dawson function,



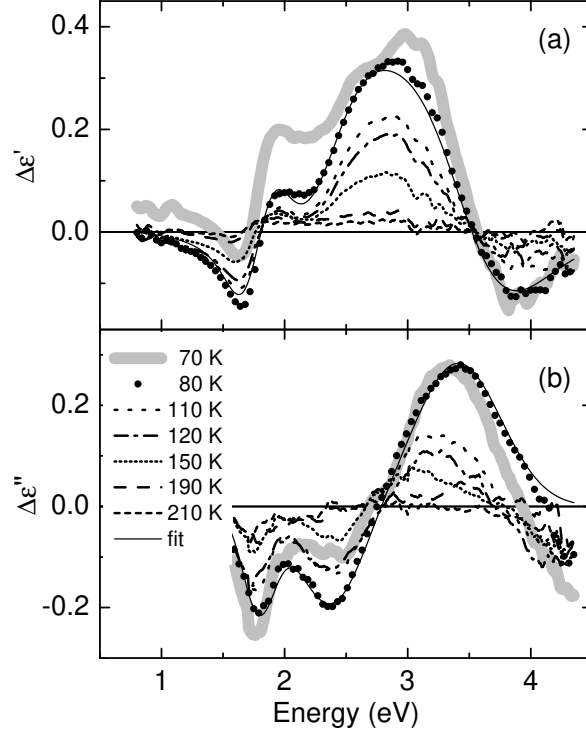


FIG. 11: The dielectric functions from Fig. 7, the real and imaginary parts, with subtracted 250 K data. The fit curve shows a simultaneous fit to the real and imaginary part for the 80 K data.

in the real part. The fitted curves for 80 K are shown along with the experimental data in Fig. 11. The full dielectric function shown in Fig. 7 was also fitted in the same way, but an additional fourth gaussian was necessary to account for the CT band. In this way the position of the bands was constrained to be temperature independent. However, it was not possible to determine accurately the absolute optical strength of the MH bands due to an additional non-gaussian contribution. It was also impossible to determine the position of the 3.3 eV band at high temperatures because of its vanishing presence in the spectra. The band positions and optical strengths obtained from the fits are plotted in Fig. 12. The dielectric function reveals minimal variations between room temperature and the second order structural phase transition at 200 K. Below 200 K a strong growth of the 3.3 eV band is observed, which is accompanied by the decrease of the 1.8 and 2.4 eV bands. The total change of the optical strength of these MH bands remains virtually zero down to the Neel temperature,  $T_N = 116$  K. In the magnetically ordered state the 3.3 eV band acquires additional strength. The additional spectral weight transfer should come from higher energies, most probably from the  $e_g$  states, as the decrease of the low energy bands

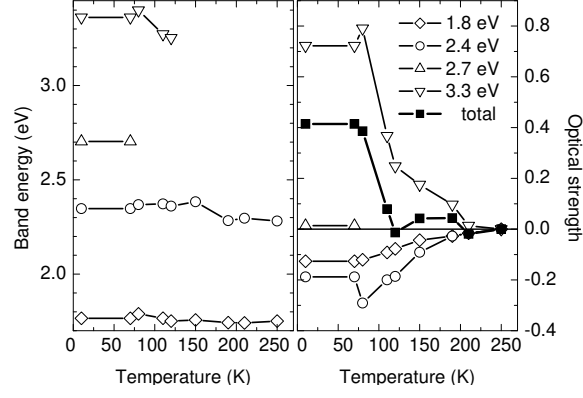


FIG. 12: Temperature dependence of the bands position (left) and their optical strength together with the total spectral weight of the three bands (right).

cannot account for it. Indeed, the lowest energy state in the  $t_{2g}^2 e_g$  configuration is obtained by adding an  $e_g$  electron to the ground state  $^3T_{1g}$ . Four irreducible representations,  $^4T_{1g}$ ,  $^4T_{2g}$ ,  $^2T_{1g}$ , and  $^2T_{2g}$  can be formed from this configuration, where the latter representation descends also from the  $t_{2g}^3$  configuration. Antiferromagnetic order favors transitions to the low-spin states and thus gives additional optical strength to the  $^2T_{2g}$  state.

At the first order phase transition, the optical strength of the 2.4 and 3.3 eV bands experiences jumps in opposite directions. Additionally, as can be seen in Fig. 11 (a), a new shoulder emerges at around 2.7 eV. This appears in Fig. 7 as an extended flat region, which becomes visible probably due to the narrowing of the 3.3 eV band. However, its optical strength is very small.

The optical spectrum begins to change below the second order phase transition at 200 K. These changes can not be directly related to the lower symmetry as the 3.3 eV band does not disappear in the low temperature orthorhombic phase. The reason should rather come from some electronic correlations and associated distortions of the  $VO_6$  octahedrons. Ren et al.<sup>2</sup> suggested that the spin order in  $YVO_3$  is accompanied by an orbital order. The orbital order is reported to appear below the 200 K phase transition<sup>4,7</sup>. In the proposed picture for the orbital ordering, the xy-orbitals are always occupied by one of the two d electrons, while the occupation of the xz and yz orbitals alternates in an AFM order. The orbital order was found to be different above and below 77 K in agreement with the different magnetic order. According to Ren et al.<sup>2</sup>, there is a C-type magnetic and G-type orbital order above 77 K, and alternatively G-type magnetic and C-type orbital order below 77 K.

We now turn to the discussion of how orbital and magnetic ordering influences the optical conductivity. We consider a model, where the optical conductivity is proportional to the electron transition probability between two neighboring vanadium sites. There are in total nine independent eigenfunctions in the  ${}^3T_{1g}$  representation. At room temperature the electron transition probability can be calculated by averaging over arbitrary orientations of spin and orbits on two ions, i.e. by averaging over all linear combinations of these 9 wave functions. Magnetic or orbital order limits the choice of the initial wave functions. At lower temperatures we can expect that the electron transition from the  $S=1$  state on the first ion to the  $S=3/2$  state on the other ion becomes less probable due to the antiferromagnetic order. Thus, the intensity of the lowest band should decrease. As can be seen from Fig. 7 and Fig. 11, the optical strength of the lowest band indeed decreases together with temperature. By using a more rigorous analysis of the transition probabilities, we can evaluate if a particular order is consistent with the observed temperature dependence for  $\text{NiO}$ . In this analysis we neglect the tilting of octahedrons, and assume that the transition integrals between d-orbitals on the neighbor vanadium ions are the same for all directions and for all d orbitals. The conductivity is assumed to be determined by the probabilities to create a pair consisting of an occupied orbital on one site and an empty orbital on the neighboring site, with the constraint that the transition is allowed. The intersite d-d transitions are mediated by the p orbitals of the oxygen ions between the vanadium sites. At room temperature all  ${}^3T_{1g}$  states are occupied randomly. At lower temperatures we used the magnetic and orbital order, suggested above<sup>2</sup>. If we assume the transition integral from completely occupied to completely empty orbital as unity, then the transition probabilities at room temperature are found to be 0.49, 0.84, and 0.44 for the  ${}^4A_{2g}$ ,  ${}^2E_g + {}^2T_{1g}$ , and  ${}^2T_{2g}$  final states, respectively. We also calculated the transition probabilities for AFM spin order and for AFM spin order accompanied by the aforementioned orbital order (see Table IV). Both simple AFM-SO and AFM-SO+OO lead to a decrease of the lowest band and an increase of the intensity of the highest band, consistent with the observations.

However, none of the considered orderings gives the correct sign for the intensity change for the middle band, i.e. a decrease of strength with decreasing temperature. Moreover, we found that no combination of completely polarized states ( $S_z = 1$ ) can give the desired intensity decrease for the  ${}^2E_g + {}^2T_{1g}$  band. The same conclusions hold if the on-site symmetry is lowered to tetragonal. If some addition of the  $S_z = 0$  initial wave function is allowed, as

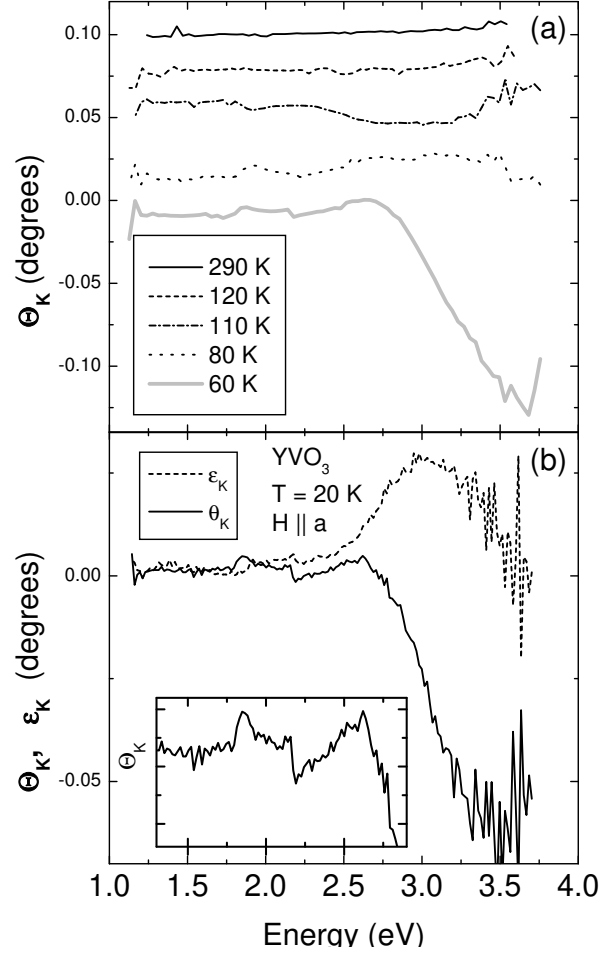


FIG. 13: (a) Temperature dependence of the Kerr rotation measured in the polar geometry with  $H \parallel a$ . (b) The Kerr rotation  $\theta_K$  together with the Kerr ellipticity  $\epsilon_K$  in the low temperature phase. (Insert) Enlarged view of the resonances at 1.8 and 2.2 eV.

suggested by neutron measurements<sup>4</sup>, a whole number of possible orbitally ordered structures becomes allowed. Although different orbital orderings can indeed explain the observed intensity changes, it is not possible to give a preference to a particular order<sup>21</sup>.

## V. MAGNETO-OPTICAL KERR EFFECT

The energy diagram shown in Fig. 9 was derived assuming a local cubic symmetry on the vanadium site. In reality, one axis of the octahedron is different from the other two. This tetragonal type distortion additionally splits the multiplet structure, which partially lifts the degeneracy of the ground and excited states. On top of that, a spin-orbital coupling

provides segregation of the states by the quantum number  $M_J$ . The latter gives rise to the magneto-optical Kerr effect (MOKE). Temperature dependence of the Kerr rotation spectrum  $\theta_K(E)$  is shown in Fig. 13. The curves are shifted for clarity. The measurements were performed in the polar geometry at nearly normal angle of incidence, with magnetic field of 0.1-0.2 T parallel to the  $a$  axis,  $H \parallel a$ . In the other field orientations, the magnetic moment was too small for the Kerr rotation to be detected. No rotation of the polarization plane was observed above the Neel temperature within our experimental error. Below the Neel temperature but above the first order phase transition, only a weak structure of the order of  $\theta_K \approx 0.01$  can be seen. Below 75 K a remarkable peak as large as  $\theta_K = 0.1$  is observed. In total, there are three resonance structures. Enlarged in the insert of Fig. 13 are two surprisingly narrow dispersion type resonances at 1.8 and 2.2 eV that have positions approximately corresponding to the onset of the two first MH bands. Their intensity, though rather small  $\approx 0.01$ , is well reproduced on different samples. The third broad peak appears to have maximum at 3.5 eV, which is also coincided by the zero crossing of the Kerr ellipticity  $\theta_K(E)$ . This band lies below the charge-transfer onset and corresponds to the  $d-d$  transitions. The maximum rotation in this band amounts to  $\approx 0.1$ . Such a large magneto-optical effect seems to be quite surprising, because from the electrodynamics point of view the time-reversal symmetry, although broken on the microscopic scale, is usually restored on the macroscopic scale in antiferromagnetic compounds. If this indeed were the case in  $YVO_3$ , the Kerr rotation would mainly result from the small 0.2 spin canting and would be as minuscule as the net magnetic moment is. For comparison, the saturation magnetic moment in Ni is  $0.61 \mu_B$  per atom, i.e. approximately 60 times larger than the net moment of 0.01 Bohr magneton per vanadium atom in  $YVO_3$ . Still the Kerr rotation in Ni is quite comparable to those of the low temperature phase of  $YVO_3$  and lies between 0.1 and 0.2 in the visible range.

Antiferromagnetic compounds can have large magneto-optical effects, as was shown recently<sup>22,23</sup>, if the local spin and orbital magnetic moments are not collinear. In particular, an orbital magnetic moment does not vanish in transition-metal perovskites with the Pbnm structure due to the tilting of the octahedra<sup>24</sup>. We can find non-vanishing ferromagnetic components of the net orbital magnetic moment  $M_L$  from symmetry considerations, following the guideline and notations from Ref. 24. There are four inequivalent vanadium sites  $i = 1; 2; 3; 4$  in the  $YVO_3$  unit cell. These sites can be generated by four symmetry

transformations, unity operation  $E$ , and three screw axes,  $S_{2x}$  with the shift  $(\frac{1}{2}, 0, 0)$  and coordinates  $x, \frac{1}{4}, 0$ ;  $S_{2y}$   $(0, \frac{1}{2}, 0)$   $\frac{1}{4}, y, \frac{1}{4}$ ; and  $S_{2z}$   $(0, 0, \frac{1}{2})$   $0, 0, z$ . Here  $x, y$ , and  $z$  are parallel to the crystallographic axes  $a, b$ , and  $c$ , respectively. The local relation between the orbital magnetic moment  $M_L^i$  and spin magnetization direction  $e = (\cos \theta \sin \phi; \sin \theta \sin \phi; \cos \theta)$  on each vanadium site  $i$  can generally be written as  $M_L^i = L^i e$ , where the matrix  $L^i$  determines the orbital magnetic moment induced by the spin-orbit interaction. We apply the mentioned symmetry operations to the matrix  $L^i$  to obtain averaged matrices  $L = \frac{1}{4} \sum_{i=1}^4 L^i$  for the C- and G-type spin ordering, respectively:

$$L^C = \frac{1}{4} \begin{pmatrix} 0 & L_{xy}^1 & 0 \\ L_{yx}^1 & 0 & 0 \\ 0 & 0 & 0 \end{pmatrix} \begin{matrix} B \\ B \\ C \\ A \end{matrix}; \quad L^G = \frac{1}{4} \begin{pmatrix} 0 & 0 & L_{xz}^1 \\ 0 & 0 & 0 \\ L_{zx}^1 & 0 & 0 \end{pmatrix} \begin{matrix} B \\ B \\ C \\ C \\ A \end{matrix}$$

The corresponding net orbital magnetic moments are

$$C : M_L^C = 4(L_{xy}^1 \sin \theta \sin \phi; L_{xy}^1 \sin \theta \cos \phi; 0);$$

$$G : M_L^G = 4(L_{xz}^1 \cos \theta; 0; L_{zx}^1 \sin \theta \cos \phi);$$

The orbital magnetic moment  $M_L$  has the same symmetry as the gyration vector  $g^{25}$ , which determines the antisymmetric part of the dielectric tensor,  $\epsilon^a = i e g$ , which is responsible for magneto-optical effects<sup>26</sup>. Here  $e$  is the unit antisymmetric tensor. In the polar measurement geometry discussed here, components of the vector  $g$  and correspondingly components of  $M_L$  define the orientation of magnetic field  $H$ , at which the observation of Kerr effect is possible.

For the G-type spin order, the structure of  $M_L^G$  suggests that the polar Kerr effect can exist for  $H \parallel a$ , if spins are parallel to the  $c$  axis, and for  $H \parallel c$ , if spins are aligned along the  $a$  axis. If the spins are along the  $b$  axis,  $M_L^G$  and the corresponding Kerr effect are zero. This does not exclude the possibility for the second, weaker, type of Kerr effect, which is directly related to the spin canting. It should be emphasized here that the Kerr rotation due to the orbital magnetic moments can exist even if spins are exactly antiferromagnetically aligned<sup>24</sup>. Our observation of the substantial magneto-optical effect only for  $H \parallel a$  shows that spins in the low temperature phase of  $YVO_3$  are aligned along the  $c$  axis. This agrees with the neutron scattering measurements<sup>4</sup>. The weak structure at 1.8 and 2.2 eV is most probably the spin canting effect.

The C-type spin order as seen from the  $M_L^C$  angular dependence allows a magneto-optical activity, only if spins are aligned in the ab plane. The small magnitude of the experimentally observed MOKE above 80 K compared to the low temperature phase suggests that the spins are aligned along the c axis. In this case,  $M_L^C$  is zero for any orientation of  $H$ , and Kerr effect substantially decreases, in agreement with the our experimental observations. This result contradicts the neutron data, where a substantial spin component along the b axis is observed<sup>4</sup>. This, however, can reflect another important property of  $YVO_3$ . As it was shown in Ref. 27, the G-type antiferromagnetic orbital order in the form proposed by Ren et. al.<sup>2</sup> suppresses the orbital magnetic moment. This can be the reason, why no substantial Kerr rotation was observed for the C-type spin order. This conclusion requires that the on-site magnetic moment in the G-type orbital order is reduced from  $2\mu_B$  to  $1\mu_B$ <sup>4</sup> not due to the orbital magnetic moment, but due to a mixture of  $S_z = 1$  and  $S_z = 0$   ${}^3T_{1g}$  states, in agreement with the conclusion obtained in the previous section.

## V I. C O N C L U S I O N S

The analysis of the  $YVO_3$  phonon spectra revealed three different phases. The orthorhombic Pbnm structure exists down to 200 K. At 200 K there is a second order phase transition to a lower symmetry structure. Orthorhombic Pbnm crystal symmetry is restored through a first order phase transition below 74 K. The most probable structure in the intermediate phase is the monoclinic Pbl1, where the  $VO_6$  octahedra form a dimerized chain along the c axis. The triclinic  $P\bar{1}$  symmetry cannot however be completely excluded.

$YVO_3$  is a Mott-Hubbard insulator with the optical gap of 1.6 eV. There are three optical bands with energies 1.8, 2.4, and 3.3 eV. We identify these bands with the inter-vanadium transitions from the  ${}^3T_{1g}$  ground state to the  ${}^4A_{2g}$ ,  ${}^2E_g + {}^2T_{1g}$ , and  ${}^2T_{2g}$  states. These d-d excitations are followed by the charge-transfer transitions at 4 eV. The band gap structure is in agreement with the LSDA+U calculations. The d bands revealed strong temperature dependence. Using a model, which includes only the nearest neighbor transitions, we found that the observed temperature dependence disagrees with the simple antiferromagnetic spin ordering. This indicates that an orbital order is responsible for the band temperature variations. However, the commonly considered  $\{xy; xz\} - \{xy; yz\}$  orbital order seems also inconsistent with our data, if we assume a fully polarized on-site state.

We observed two types of magneto-optical effect. Small net magnetic moment due to the uncompensated spin moments induces the weak Kerr rotation of the order of  $0.01^\circ$ . The effect exists in all phases below the magnetic ordering temperature and for all active optical transitions. A strong Kerr effect appears as a consequence of the low crystallographic symmetry and ferromagnetic ordering of orbital magnetic moments. The Kerr rotation of the order of  $0.1^\circ$  was found in the low temperature phase for the highest d-d transition band. It follows from the symmetry considerations that the spin magnetic moment lays along the c axis in both magnetic structures. However, this conclusion for the C-type AFM spin arrangement can be affected by the accompanying orbital order.

#### Acknowledgments

We acknowledge useful discussion with G. R. Blake. We thank H. J. Bron for his help with sample preparation. This research was supported by the Netherlands Foundation for Fundamental Research on Matter (FOM) with financial aid from the Nederlandse Organisatie voor Wetenschappelijk Onderzoek (NWO).

---

Present address: NSRIM Institute, University of Nijmegen, Toernooiveld 1, 6525 ED Nijmegen, The Netherlands; Electronic address: tsvetkov@sci.kun.nl

<sup>y</sup> On leave from Jurusan Fisika, Institut Teknologi Bandung, Jl. Ganesha 10, Bandung 40132, Indonesia.

<sup>1</sup> K. I. Kugel and D. I. Khomskii, ZhETF 64, 1429 (1973), [Sov. Phys. JETP 37, 725 (1973)].

<sup>2</sup> Y. Ren, T. T. M. Palstra, D. I. Khomskii, E. Pellegrin, A. A. Nugroho, A. A. Menovsky, and G. A. Sawatzky, Nature 396, 441 (1998).

<sup>3</sup> H. Kawano, H. Yoshizawa, and Y. Ueda, J. Phys. Soc. Jpn. 63, 2857 (1995).

<sup>4</sup> G. R. Blake, T. T. M. Palstra, Y. Ren, A. A. Nugroho, and A. A. Menovsky, Phys. Rev. B 65, 174112 (2002).

<sup>5</sup> D. B. Rogers, A. Ferretti, D. H. Ridgley, R. J. A. Mott, and J. B. Goodenough, J. Appl. Phys. 37, 1431 (1966).

<sup>6</sup> V. G. Zubkov, A. S. Borukhovich, G. V. Bazuev, I. I. Matveenko, and G. P. Shveikin, Sov.



- Phys. JETP 39, 896 (1974).
- <sup>7</sup> G . R . B lake, T . T . M . P alstra, Y . R en, A . A . N ugroho, and A . A . M enovsky, Phys. Rev. Lett. 87, 245501 (2001).
  - <sup>8</sup> C . U lrich, G . K haliullin, J . S irker, M . R eehuis, M . O hl, S . M iyasaka, Y . T okura, and B . K eim er (2002), cond-m at 0211589.
  - <sup>9</sup> Y . R en, T . T . M . P alstra, D . I . K hom skii, A . A . N ugroho, A . A . M enovsky, and G . A . S awatzky, Phys. Rev. B 62, 6577 (2000).
  - <sup>10</sup> K . S ato, H . H ongu, H . I kekam e, Y . T osaka, M . W atanabe, K . T akanashi, and H . F ujim ori, Jpn. J. Appl. Phys. 32, 989 (1993).
  - <sup>11</sup> D . L . R ousseau, R . P . B aum an, and S . P . S . P orto, J. Ram an Spec. 10, 253 (1981).
  - <sup>12</sup> A . A . T svetkov, F . P . M ena, Y . R en, I . S . E l m ov, P . H . M . van Loosdrecht, D . van der M arel, A . A . N ugroho, A . A . M enovsky, and G . A . S awatzky, Physica B 312, 783 (2002).
  - <sup>13</sup> I . S . S m imova, Physica B 262, 247 (1999).
  - <sup>14</sup> S . M iyasaka, Y . O kin oto, and Y . T okura, J. Phys. Soc. Jpn. 71, 2086 (2002).
  - <sup>15</sup> J . Z aanen, G . A . S awatzky, and J . W . A llen, Phys. Rev. Lett. 55, 418 (1985).
  - <sup>16</sup> M . K asuya, Y . T okura, T . A rim a, H . E isaki, and S . U chida, Phys. Rev. B 47, 6197 (1993).
  - <sup>17</sup> T . A rim a, Y . T okura, and J . B . T orrance, Phys. Rev. B 48, 17006 (1993).
  - <sup>18</sup> O . K . A ndersen, Phys. Rev. B 12, 3060 (1975).
  - <sup>19</sup> V . I . A n isim ov, J . Z aanen, and O . K . A ndersen, Phys. Rev. B 44, 943 (1991).
  - <sup>20</sup> H . S awada and K . T erakura, Phys. Rev. B 58, 6831 (1998).
  - <sup>21</sup> (????), for exam ple, if we m axim ize the spin m agnetic m om ent, we obtain that the  $\uparrow z, \uparrow yz$  orbitals should be always occupied on all vanadium sites. This gives correct intensity changes for the all bands and all axes.
  - <sup>22</sup> I . V . S olovyev, N . H am ada, and K . T erakura, Phys. Rev. Lett. 76, 4825 (1996).
  - <sup>23</sup> L . M . S andratskii and J . K ubler, Phys. Rev. Lett. 76, 4963 (1996).
  - <sup>24</sup> I . V . S olovyev, Phys. Rev. B 55, 8060 (1997).
  - <sup>25</sup> Y . A . U spenskii, E . T . K ulatov, and S . V . H alilov, Phys. Rev. B 54, 474 (1996).
  - <sup>26</sup> D . L . L andau and E . M . L ifshitz, E lectrodynam ics of C ondensed M edia (Pergam on, New York, 1960).
  - <sup>27</sup> T . J o, J. Phys. Soc. Jpn. 72, 155 (2003).

TABLE II: c-Axis phonons at 75 K.  $B_{2u}$  modes originate from the room temperature phase. New vibrational modes, appearing below 200 K, are designated as A

M ode	F reque ncy	$S_a$	$S_b$	$S_c$
$B_{2u}$	180.2			7
A	199		0:037	0:008
$B_{2u}$	205.6		0:006	0:78
$B_{2u}$	333.0	0:19	0:008	2:9
A	350		0:67	0:003
$B_{2u}$	359.8		0:02	0:37
$B_{2u}$	420.5	1:6	0:076	1:6
A	522		0:024	0:018
$B_{2u}$	564.9		0:014	1:2
$B_{2u}$	699.2			0:002

TABLE I: TO phonon modes for the a and b axes at room temperature.

$B_{1u}$ (a)			$B_{3u}$ (b)		
$\omega$ , $\text{cm}^{-1}$	$\omega$ , $\text{cm}^{-1}$	$S_a$	$\omega$ , $\text{cm}^{-1}$	$\omega$ , $\text{cm}^{-1}$	$S_b$
162.2	3:2	0:08	144.3	15:5	0:73
211.6	8:5	5:4	237.4	5:5	2:0
328.5	9:9	1:6	280.1	8:4	0:64
359.2	15:0	0:56	318.7	7:8	0:35
420.8	10:4	1:4	374.5	6:3	0:22
446.8	17:3	2:6	390.7	16:5	4:21
494.5	10:0	0:005	471.7	13:3	1:2
517.5	15:5	0:06	543.7	9:8	0:86
572.4	22:6	0:91	559.8	17:5	0:21

TABLE III: Possible symmetries and symmetry operations in the intermediate phase ( $75\text{K} < T < 200\text{K}$ ).

N	P nm a	P bnm	P 2 <sub>1</sub> =a	P $\bar{1}$	P b11
	D <sub>2h</sub> <sup>16</sup>	D <sub>2h</sub> <sup>16</sup>	C <sub>2h</sub> <sup>5</sup>	C <sub>i</sub> <sup>1</sup>	C <sub>s</sub> <sup>2</sup>
(1)	1	1	1	1	1
(2)	2 (0;0; $\frac{1}{2}$ ) $\frac{1}{4}$ ;0;z	2 ( $\frac{1}{2}$ ;0;0) x; $\frac{1}{4}$ ;0	2 <sub>1</sub>	—	—
(3)	2 (0; $\frac{1}{2}$ ;0) 0;y;0	2 (0;0; $\frac{1}{2}$ ) 0;0;z	—	—	—
(4)	2 ( $\frac{1}{2}$ ;0;0) x; $\frac{1}{4}$ ; $\frac{1}{4}$	2 (0; $\frac{1}{2}$ ;0) $\frac{1}{4}$ ;y; $\frac{1}{4}$	—	—	—
(5)	{	{	{	{	—
(6)	a x;y; $\frac{1}{4}$	b $\frac{1}{4}$ ;y;z	b	—	b
(7)	m x; $\frac{1}{4}$ ;z	m x;y; $\frac{1}{4}$	—	—	—
(8)	n (0; $\frac{1}{2}$ ; $\frac{1}{2}$ ) $\frac{1}{4}$ ;y;z	n ( $\frac{1}{2}$ ;0; $\frac{1}{2}$ ) x; $\frac{1}{4}$ ;z	—	—	—

TABLE IV: Calculated transition probabilities at room temperature, in the AFM spin ordered (SO) state and in the AFM spin and orbital ordered (SO-OO) state.

Order	<sup>4</sup> A <sub>2g</sub>	<sup>2</sup> E <sub>g</sub> + <sup>2</sup> T <sub>1g</sub>	<sup>2</sup> T <sub>2g</sub>
Room temperature	0.49	0.84	0.44
AFM SO	0.30	1.48	0.89
AFM SO-OO	0.33	1.67	1.0